Research Article | Vol. 13, No. 2 / 1 Feb 2022 / Biomedical Optics Express 995
Biomedical Optics EXPRESS

Spectral focusing in picosecond pulsed stimulated Raman scattering microscopy

KOTA KOIKE,[1,2] NICHOLAS I. SMITH,[3] AND KATSUMASA FUJITA[1,2,4,*]

[1]Department of Applied Physics, Osaka University, 2-1 Yamadaoka, Suita, Osaka 565-0871, Japan
[2]AIST-Osaka University Advanced Photonics and Biosensing Open Innovation Laboratory, National Institute of Advanced Industrial Science and Technology (AIST), 2-1 Yamadaoka, Suita, Osaka 565-0871, Japan
[3]Immunology Frontier Research Center, Osaka University, 2-1 Yamadaoka, Suita, Osaka 565-0871, Japan
[4]Transdimensional Life Imaging Division, Institute for Open and Transdisciplinary Research Initiatives, Osaka University, 2-1 Yamadaoka, Suita, Osaka 565-0871, Japan
*fujita@ap.eng.osaka-u.ac.jp

Abstract: We introduce spectral focusing of picosecond laser pulses in stimulated Raman scattering (SRS) microscopy to improve spectral resolution, reduce nonlinear background signals, and decrease nonlinear photodamage. We produce a pair of 14 ps pump and Stokes laser pulses by spectral focusing of a 2 ps laser and achieve a spectral resolution of 2 cm^{-1}. Due to instantaneous narrow-band excitation, we find that the chirped 14 ps laser pulses can be used to improve the signal-to-background ratio in SRS microscopy of various samples such as polymer particles and small molecules in HeLa cells. The lower peak powers produced by chirped picosecond laser pulses also reduce nonlinear photodamage, allowing long-term SRS imaging of living cells with higher SNR.

1. Introduction

Stimulated Raman scattering (SRS) is based on an energy transfer mechanism in a sample between two laser pulses, called pump and Stokes beams. When the beat frequency of the two beams matches a specific vibration frequency of the sample, a portion of the pump beam energy is transferred to the Stokes beam. Compared to spontaneous Raman scattering, the strength of the SRS process and resulting signals can be enhanced by a factor of more than 10^5. This enhancement has been exploited to allow high-speed vibrational imaging of biological samples [1–3]. Recent developments of small Raman probes have increased the degree of multiplexed detection available in vibrational imaging of cellular organelles [4,5]. Multiplexing, however, increases the density of Raman peaks, which can become separated by only 10-20 cm^{-1}, thus requiring higher spectral resolution to resolve each peak. This then leads to a compromise: while the SRS generation process is itself nonlinear and shorter pulses can produce higher signal intensities [6], longer pulse widths in the picosecond regime can actually prove advantageous for this type of application due to higher spectral resolution. Longer pulse widths can also reduce the contribution of nonlinear backgrounds, such as cross-phase modulation (XPM) to the signals [7], and reduce nonlinear photodamage due to lower excitation peak power. Aside from signal strength concerns, reducing photodamage is also essential in multiplexed or live-cell/tissue imaging applications. However, to the best of our knowledge, this regime (especially for picosecond pulses > 10 ps) has not been explored in terms of signal-to-noise ratio (SNR), signal-to-background ratio (SBR), and for the potential to allow increased sensitivity and reduced photodamage. These are all particularly important for applications in biological sample imaging, where SRS has proven to be highly useful.

#445640 https://doi.org/10.1364/BOE.445640
Journal © 2022 Received 15 Oct 2021; revised 14 Dec 2021; accepted 20 Dec 2021; published 27 Jan 2022

Biomedical Optics EXPRESS

Here, we report the application of spectral focusing to 2 ps laser pulses in intensity modulation-based SRS microscopy, stretching the pulse width to 14 ps. As a result, imaging can be achieved with a spectral resolution of 2 cm^{-1}, with lower background signals from nonlinear optical effects, and with reduced nonlinear photodamage in live-cell imaging. Single-grating-based pulse chirpers [8] are incorporated to chirp both pump and Stokes laser pulses. We demonstrate that SRS imaging can be achieved in this manner on diamond crystals, polystyrene (PS) beads, and small molecules (EdU) in HeLa cell samples, with higher spectral resolution in the longer pulse width regime. We also show that, in line with theory, longer pulse widths do improve the SBR in SRS measurements due to decreased nonlinear background and higher spectral resolution without applying frequency-modulation [9–11] or polarization-modulation schemes [12]. Our findings can be readily applied to the widely used intensity modulation SRS setups with 2 ps laser systems and exploited in applications that require high sensitivity, suppressed background, and low photodamage.

2. Experimental setup

2.1. SRS microscope with single-grating chirpers

Figure 1(a) shows a schematic of an SRS microscope equipped with two pulse chirping systems. A mode-locked Yb-fiber laser (Emerald Engine, APE) provided an output 2 ps laser pulse at 1031 nm with a repetition rate of 80 MHz and was used as a Stokes beam for SRS imaging. A wavelength-tunable laser pulse emitted from OPO (Levante Emerald, APE) with a wavelength of 660 to 990 nm was used as a pump beam for SRS imaging. The intensity of the Stokes beam was modulated by EOM (APE) at 20 MHz. A motorized-optical delay stage (M-531.DD, PI) was placed to ensure the temporal overlap between the Stokes and pump pulse trains. Both laser beams were introduced into the chirp systems individually, where the pulse widths can be easily switched between 2 (no-chirp), 7, and 14 ps. As for the 2 ps mode, the laser was reflected by a retroreflector (RF, HRS1015-AG, Thorlabs) and picked off by a mirror (PM, BBD1-EO3, Thorlabs). For the 7 and 14 ps modes, the combination of transmission gratings (Grating 1; T1400-800, Grating 2: T1000-1040, LightSmyth) mounted on movable stages (M-LNS-1, Newport) and RFs enabled the spectral focusing of picosecond pulses. The delay line position was optimized every time the pulse width and wavelength used for the imaging were changed (see Fig. S1 for detail). The overall efficiency (throughput of average power) of each chirper was around 78% for the pump (847 nm) and 83% for the Stokes beam, respectively. The diffraction efficiency of each grating was around 94% for the pump and 95% for the Stokes beam, which indicates that there was no significant power loss in other components. The beams were spatially combined after the chirper. An autocorrelator (pulseCheck SM2000, APE) was used to measure the pulse width. Laser scanning was performed by a scan unit consisting of a 2D galvanometer mirror and scan/tube lenses before an entrance port of the microscope body (ECLIPSE Ti, Nikon). Water immersion objective lenses (Plan Apo IR 60×, 1.27 NA, Nikon) were used for focusing and collecting the beams. Two identical optical bandpass filters (FF01-850/310-25, Semrock) blocked the Stokes beam. A large-area silicon photodiode (PD, S3590-09, Hamamatsu Photonics) was used as a detector. The voltage from the PD was sent to a fast lock-in amplifier (UHFLI, Zurich Instruments) for demodulation of SRS signals. The imaging parameters for all measurements are summarized in Table S1 and S2 in the Supplement 1.

We characterized the pulse width by observing the autocorrelation functions of the pump (906.6 nm) and Stokes beams (Fig. 1(b)). The pulse widths without spectral focusing (2 ps mode) were measured to be 1.79 and 1.96 ps for the pump and Stokes beams, respectively, based on the full-width-at-half-maximum (FWMH) of $sech^2$ fitting functions. The theoretical chirped-pulse width was obtained from the measured unchirped pulse width and group delay dispersion (GDD) [13]. Hence, the pulse width was adjusted by varying GDD values. The GDD value can be controlled by the distance L between a grating and retroreflector [8,14]. For the 7 ps mode, L was

Biomedical Optics EXPRESS

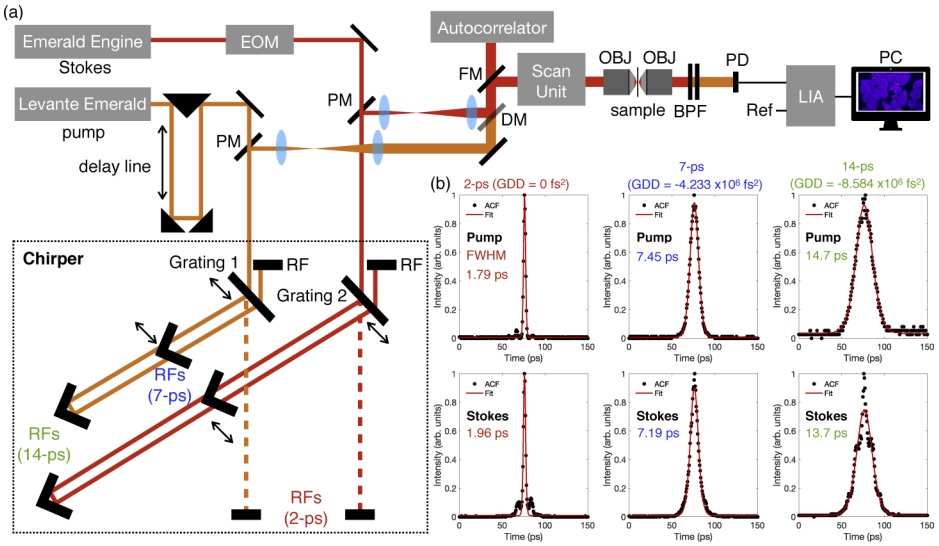

Fig. 1. An SRS microscope with picosecond pulsed spectral focusing using a single-grating-based chirp system. (a) Optical setup of SRS microscopy. EOM for electro-optic modulator; PM for pick-off mirror; RF for retroreflector; DM for dichroic mirror; FM for flip mirror; OBJ for objective lens; BPF for optical bandpass filter; PD for photodiode; Ref. for reference signal; LIA for lock-in amplifier. (b) Autocorrelation measurement of pump and Stokes laser pulses with different GDDs. The black dots are the measured values, and red line is the sech^2 fitting function.

set to be 20 (for the pump beam) and 40 cm (for the Stokes beam) with GDD of -4.233×10^6 fs^2, while the respective pulse widths were estimated to be 6.8 and 6.3 ps. For the 14 ps mode, L was calculated to be 41 and 81 cm with GDD of −8.584×10^6 fs^2, providing the pulse widths of 13.4 and 12.3 ps for pump and Stokes beam, respectively. The measured pulse widths of the pump and Stokes beams after spectral focusing were 7.45 and 7.19 ps in the 7 ps mode and 14.7 and 13.7 ps in the 14 ps mode, in good agreement with the theoretical values.

2.2. Spectral resolution

The improvement of the spectral resolution by spectral focusing was confirmed by measuring diamond crystals. Diamond crystals have a sharp Raman peak at 1332.5 cm^{-1} with a spectral width of 1.7 cm^{-1} [15,16]. The crystals (IRM2-4, Tomei Diamond) with a diameter of several micrometers were immersed in water and sandwiched between two coverslips. SRS signals at each wavenumber were acquired while changing the pump beam wavelength from 904.8 to 908.4 nm. As expected, the spectral widths in the 7 and 14 ps modes became narrower than that in the 2 ps mode (Fig. 2). The experimental and theoretical spectral resolutions were calculated based on the measured SRS spectral widths and pulse widths [13,17], and the time-bandwidth product of sech^2 pulse shape. The experimental and theoretical values of 2 ps pulses were well matched with 11.18 and 11.26 cm^{-1}. As for chirped pulses, the experimental and theoretical values were 4.12 and 2.87 cm^{-1} for the 7 ps mode, and 1.97 and 1.49 cm^{-1} for the 14 ps mode, respectively. A 30-40% difference in the chirped pulses may be due to the existence of higher order dispersion in the unchirped 2 ps laser pulses (seen as side-lobes in Fig. 1(b)). Finally, at the 14 ps pulse width regime, created by spectral focusing of a 2 ps laser source, we achieved a spectral resolution of 2 cm^{-1}, which is sufficient for resolving Raman bands of typical biological samples.

Biomedical Optics EXPRESS

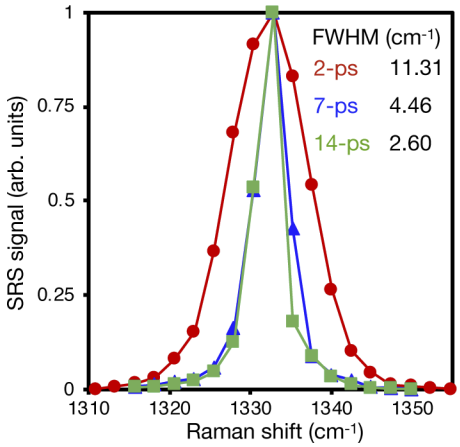

Fig. 2. Observed SRS spectra of diamond particles with different pulse widths. FWHMs of the SRS spectral widths were calculated from the Lorentzian fitting function.

3. Experimental results

3.1. Picosecond spectral focusing for multi-peak spectral resolving and improving image contrast

Next, we investigated how picosecond spectral focusing affects the spectral shape of multiple peaks and image contrast by way of SBR and SNR. Polystyrene (PS) beads were used as samples; the PS beads have two sharp Raman peaks at 1583 and 1602 cm^{-1} assigned to C=C stretch and ring-skeletal stretch modes [18]. Figure 3(a) shows SRS images obtained with 2 and 14 ps modes with the same SRS signal level at 1603.3 cm^{-1}. At a Raman shift of 1590.5 cm^{-1}, approximately halfway between the two Raman peaks, the signal decreased in the 14 ps mode due to the higher spectral resolution, whereas the 2 ps mode showed higher signal levels because the two Raman band shoulders were simultaneously excited. Because of this low spectral resolution, the two Raman peaks were not clearly resolved in the 2 ps SRS spectrum (Fig. 3(b)). The off-resonance signal intensities around 1570 and 1620 cm^{-1} were higher in the 2 ps mode than the 14 ps mode. This background signal can be derived from two factors; on-resonance excitation of the peak shoulder due to the broad excitation spectrum, and an increase of nonlinear optical effects such as the cross-phase modulation (XPM) intensity due to short pulse width and higher peak power [7]. Therefore, the observed signal at 1603.3 cm^{-1} with a longer pulse width contains a more genuine SRS signal with fewer background artifacts, which leads to higher SBR.

We further investigated the relationship between the on-resonance signal at the peak (SRS-on, 1603.3 cm^{-1}) and the off-resonance background signal (SRS-off, 1572.7 cm^{-1}) with different peak powers and pulse widths. In this experiment, the ratio of the pump beam to the Stokes beam power was kept at 1:2, and the maximum peak powers were below the damage threshold (i.e., no damage or destruction of the sample observed after 30 consecutive images). Figure 4(a) shows the relationship between SRS-on/off signals and the product of excitation peak powers. Under the same peak power, a larger SRS signal was observed at longer pulse widths due to higher average power [19]. A saturation of SRS in the 7 and 14 ps modes was observed at higher SRS signal levels, and the signals did not follow a linear relationship. This was caused by the less population difference between ground and vibrational states due to strong vibrational excitation. The SRS-off signal, mainly derived from XPM and small on-resonance excitation of the peak shoulder, also showed a linear response. Although the refractive index change experienced by the pump beam can be determined by the electric field of the Stokes beam [10,12], this result

Biomedical Optics EXPRESS

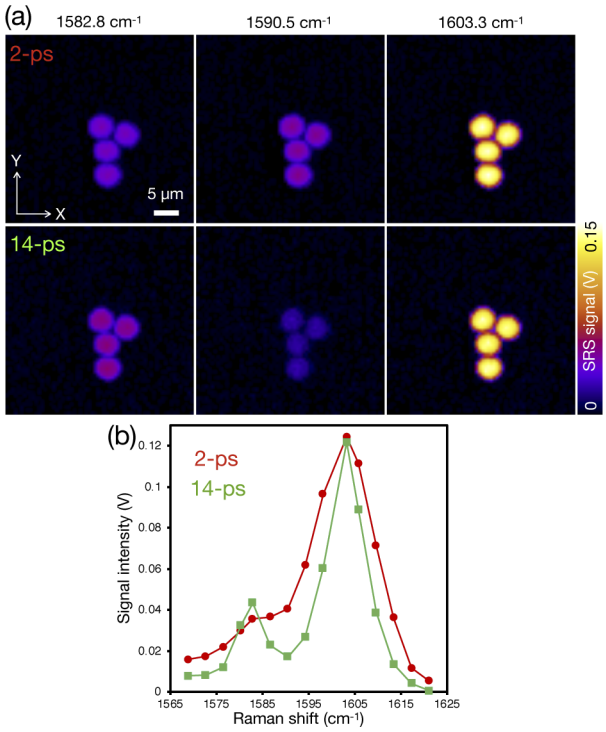

Fig. 3. Spectral focusing effects on spectral resolving of multi-peak evaluated in SRS imaging of 4.5 μm PS beads. (a) SRS images obtained at 1582.8 (C=C stretch), 1590.5, and 1603.3 cm^{-1} (ring-skeletal stretch) with 2 (red) and 14 ps (green). Scale bar, 5 μm. (b) SRS spectra of mean signal intensity from four beads with 2 (red) and 14 ps (green).

indicates that the final XPM signal amount was also affected by the pump beam intensity [20]. Based on the SRS-on/off images, SBR and SNR under different peak powers and pulse widths were calculated based on the following equations [21,22],

$$SBR = \frac{I_{ON}}{I_{OFF}} \tag{1}$$

$$SNR = \frac{I_{ON} - I_{OFF}}{\sigma_{ON}} \tag{2}$$

where I_{ON} and I_{OFF} were the PS beads signal intensity of the SRS-on and SRS-off images, respectively, and σ_{ON} was the standard deviation of the upper region of the SRS-on image without PS beads. In the SBR calculation, the background signal was assumed to be the off-resonant intensity. This can be considered as artifacts from other nonlinear optical effects overlapping with genuine SRS signals. In SNR, the prominent noise was assumed to be shot-noise, which was estimated from the pixel intensity fluctuation of the image. Even with longer pulse widths, SNR comparable to the 2 ps mode was observed using lower peak powers (Fig. 4(b)). A larger SNR can be obtained with faster scanning speed and higher average powers by reducing photothermal damage. From Eq. (1), SBR should not depend on peak powers (or SNR). However, in all pulse widths, a trade-off between SNR and SBR was observed. This might be due to the evolution of the SRS-off signal (nonlinear background signal) with increasing peak powers, and the saturation of the SRS signal at higher peak power (Fig. 4(a)), resulting in a slight decrease in SBR (= the ratio of SRS-on to SRS-off signals). However, SBR for the 14 ps remained the highest out of all

Biomedical Optics EXPRESS

pulse widths, at any given level of SNR, reaching a factor of around two compared to 2 ps. This was because that the beat frequency of chirped laser pulses was highly concentrated at the peak and thus produced a strong SRS signal. Also, due to higher spectral resolution, the off-resonance image contained less nonlinear background signal and on-resonance signal excited from the peak shoulder. To confirm this, we simulated the SRS spectrum and calculated the SBR based on the convolution of the Raman spectrum with a Lorentzian function and the laser excitation spectrum with a Gaussian function. This mathematical model also suggested that increasing the pulse width can improve SBR by a factor of 1.2-2.6, depending on the Raman peak width (Fig. S2), which agrees with the experimental results. Using chirped 14 ps pulse width, higher spectral resolution and SBR were observed while maintaining the same SNR level as the 2 ps mode.

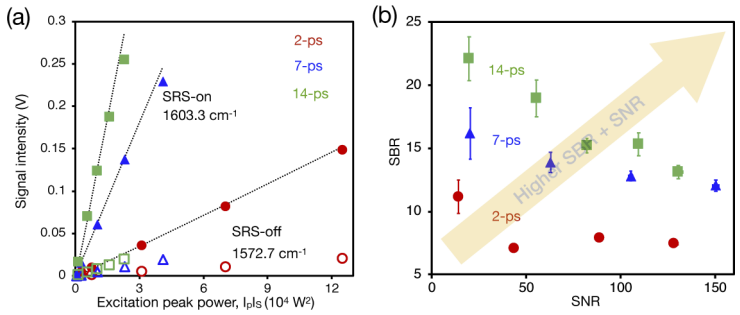

Fig. 4. Spectral focusing effects on signal-to-noise (SNR) and signal-to-background ratios (SBR) were evaluated in SRS imaging of 4.5 μm PS beads. (a) Relationship between the mean signal intensity and the product of peak powers of pump and Stokes beams. The closed and open dots represent the SRS-on and SRS-off signal values at the respective pulse widths. Dashed line of each pulse width represents a fitting curve with a power of 1. N=4. (b) Relationship between SNR and SBR. Error bar, standard deviation. N=4.

3.2. *Alkyne-tag small molecule imaging with improved signal-to-background ratio*

One possible future application of this technique is multiplex SRS imaging in cells based on the 2 ps laser system, where reduction of nonlinear background and high spectral resolution are strongly required. To evaluate whether spectral focusing with picosecond pulses based on the 2 ps laser system and whether the physical relationships discussed above produce practical benefits for such applications, we performed SRS imaging/spectroscopy of EdU in HeLa cells with 2 and 14 ps modes. The cells were cultured with serum-free DMEM for 24 h to synchronize the cell cycle [23]. Then, the cells were cultured with DMEM containing EdU 100 μM for another 24 h. The cells were chemically fixed by PBS with PFA 4% before imaging. In order to achieve the same signal level from the cells, the average power of the pump and Stokes beams was set to 25 and 50 mW, respectively, in the 2 ps mode, and 60 and 120 mW in the 14 ps mode. Hence, the peak powers were 3 times smaller in the 14 ps mode. The SRS image of CH_3-stretching mode in Fig. 5(a) was measured to locate the cells. The SRS signal of EdU inside the cell nucleus was observed with both 2 and 14 ps modes at 2117 cm^{-1} (Fig. 5(b)). Away from the peak at 2109 and 2101 cm^{-1}, the SRS signals of EdU decreased, leaving only nonlinear background signals with no Raman resonance. Both 2 and 14 ps showed similar SRS signal intensity of around 2.5×10^{-3} V at 2117 cm^{-1} (Fig. 5(c)). In the 2 ps mode, the signal intensity at 2101 cm^{-1} was still around 1.5×10^{-3} V. This indicates that the 2 ps SRS signal was largely comprised of the nonlinear background signals such as XPM, rather than genuine SRS signal of EdU. Figure 5(d) shows the reference SRS spectra of EdU powders. The 14 ps SRS spectrum showed a narrower spectral width of 9 cm^{-1}. Therefore, the SRS signal of EdU in the cells dropped rapidly at 8 cm^{-1} away from the peak with fewer nonlinear background signals. (Fig. 5(c)). This indicates that the 14 ps

Biomedical Optics EXPRESS

SRS image at 2117 cm^{-1} contained more SRS from EdU. We then subtracted the pixel value of the off-resonant image (at 2101 cm^{-1}) from the pixel value of the on-resonant image (at 2117 cm^{-1}) to remove the nonlinear background signals and calculate the true SRS subtraction image [9,24]. Indeed, the subtraction EdU image of 14 ps showed a higher SRS signal level than that of 2 ps (Fig. 5(e)). These results highlight the strong potential of SRS microscopy with spectral focusing of picosecond laser pulses in small molecule imaging in a complex biological sample with higher spectral resolution and background suppression capability.

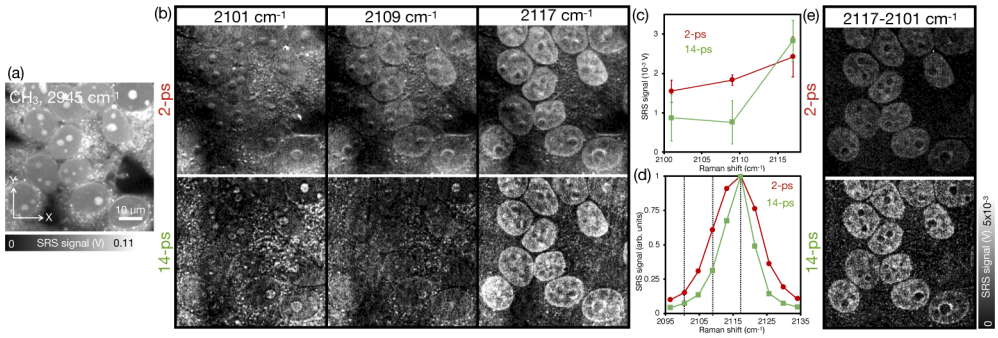

Fig. 5. SRS imaging of EdU in HeLa cells with 2 and 14 ps laser pulses. (a) SRS image of CH_3-stretching mode to locate the cell positions by 2 ps laser pulses. (b) SRS images at different wavenumbers around the alkyne peak with 2 (red) and 14 ps (green). Five images were continuously acquired, and the averaged images are shown. The brightness is the same. (c) Mean signal intensity of cell nucleus regions at each wavenumber with 2 (red) and 14 ps (green). Error bar, standard deviation. N = 12. (d) Reference SRS spectra of EdU powders with 2 (red) and 14 ps (green), normalized by the SRS peak intensity. Black dot lines indicate the wavenumbers at 2101, 2109, and 2117 cm^{-1}. (e) Subtraction SRS images between 2117 and 2101 cm^{-1} with only EdU contrast. The brightness is the same.

3.3. *Time-lapse imaging of living cells with reduced nonlinear photodamages*

To apply SRS microscopy for live-cell imaging, nonlinear photodamage processes such as two-photon absorption and coherent Raman-induced absorption [25,26] by two laser pulses with intense peak power should be considered and minimized. We thus evaluated the photodamage in the 2 ps SRS imaging and compared it with spectral focusing. To characterize the photodamage, we performed time-lapse observation of living HeLa cells and continuously acquired SRS images of the CH_3-stretching mode (2940 cm^{-1}) over 100 frames with 1 s/frame. With low average powers (low SNR conditions), no significant difference in nonlinear photodamage was observed between the different pulse width modes, which indicates that all pulse width modes were below the damage threshold (Fig. S3). Then, we increased the average powers by 2 to 2.5 times and evaluated the photodamage in the same way. To realize the same SNR levels, the pump and Stokes average powers on sample were set to 30 and 60 mW for 2 ps, 75 and 150 mW for 7 ps, and 95 and 190 mW for 14 ps, respectively. In 2 ps mode, the onset of cellular membrane breakdown appeared during the imaging (Fig. 6(a)), and then SNR rapidly decreased (Fig. 6(b)). On the other hand, in the 7 and 14 ps modes, no significant change in the appearance of the cells was observed. The SNRs were still higher levels with only 25% and 17% decrease compared to the first frame. The peak powers used in the 7 and 14 ps modes were about 1.4 and 2.2 times lower than the 2 ps mode, respectively. Therefore, nonlinear photodamages such as two-photon absorption and Raman-induced absorption could be also reduced [26], and in the parameters used here, the 2 ps excitation shows a higher probability to exceed the nonlinear damage threshold. SRS imaging with chirped picosecond pulses reduced not only nonlinear background contributions but also

Biomedical Optics EXPRESS

nonlinear photodamage, and thus has potential for long-term observation of living cells under physiological conditions.

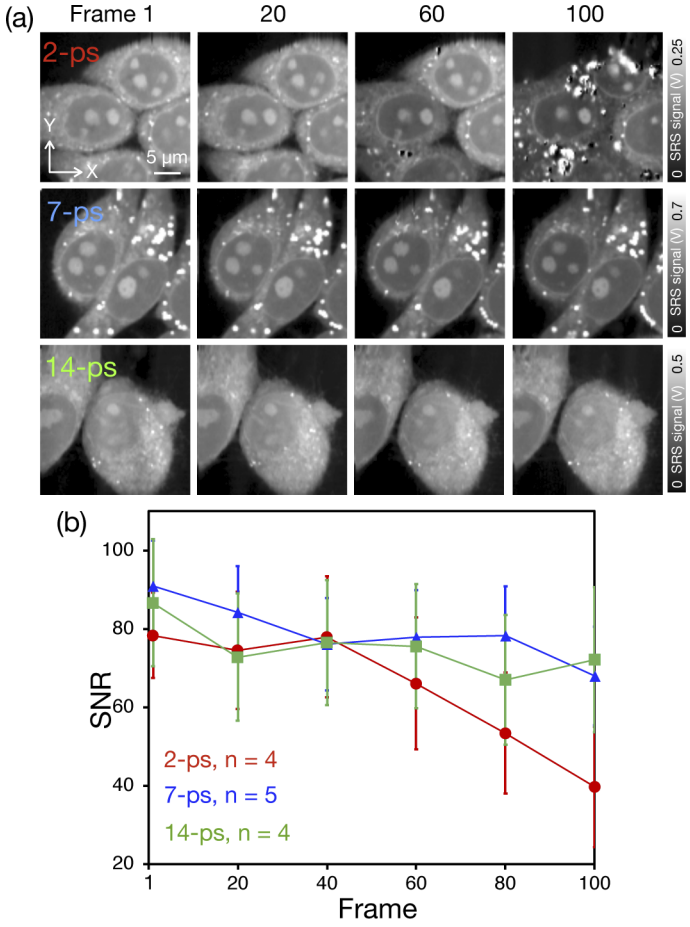

Fig. 6. Time-lapse SRS imaging of living HeLa cells with 2, 7, and 14 ps laser pulses. (a) SRS images of the cells at each frame with 2 (red), 7 (blue), and 14 ps modes (green). Scale bar, 5 μm. (b) Time (frame)-dependence of SNRs at different pulse widths. Error bar, standard deviation.

4. Conclusion

In this study, we determined that SRS imaging with spectral focusing allows high spectral resolution with nonlinear background and photodamage suppression capabilities, and is directly applicable in intensity modulation SRS microscopy. In the 14 ps mode, we have achieved a spectral resolution of 2 cm^{-1}, closely matched with the theoretical value. We also experimentally and theoretically found that the narrow instantaneous excitation bandwidth of chirped picosecond pulses reduces both the non-resonant nonlinear background and the on-resonance excitation of Raman peak shoulder, resulting in higher SBR by a factor of around two. These properties enabled the use of alkyne-tagged small molecules for intracellular imaging, with higher spectral resolution and SBR. Other detection schemes for background-free SRS, such as frequency modulation [9–11] and polarization modulation [12], have also been proposed. The spectral focusing approach presented here can be easily adopted in these non-intensity modulation

Biomedical Optics EXPRESS

schemes, further improving image contrast. Thanks to the reduced peak powers in chirped picosecond laser pulses, higher SNRs and cellular structures were maintained without significant nonlinear photodamages during time-lapse imaging. Note that to obtain the same SNR levels, 2.3 and 3.7 times higher average powers can be required in the 7 and 14 ps modes, respectively [19]. This power level is still lower than the peak power of the 2 ps mode, allowing long-term SRS imaging with higher SNR and reduced photodamages.

The spectral focusing technique was initially applied to the femtosecond laser system to perform hyperspectral SRS imaging with 100-300 cm^{-1} by delay line tuning [17,27,28]. Due to the limited bandwidth of the 2 ps laser pulses (< 1 nm of FWHM), we tuned the wavelength of the pump beam and delay line position for each SRS image for hyperspectral imaging (Fig. S1). The wavenumber range in the present system for each hyperspectral imaging was limited to 60-70 cm^{-1} due to the size of the retroreflector and grating. However, owing to the high spectral resolution of 2 cm^{-1}, it would be possible to increase the number of Raman peaks (or Raman probes) in this narrow spectral region to observe multiple cellular organelles with higher image contrast and spectral resolution. The developed pulse chirper is also applicable for the fs laser pulses since the physical principles are the same as that of conventional dual-grating geometry. In addition, the system can be more compact for fs pulses because the distance between the grating and retroreflector required for fs spectral focusing is shorter than that for picosecond laser pulses. For example, for a 200-fs laser pulse at 1031.2 nm, the distance required to stretch the pulse width to 14 ps is only 10 cm. A spectral range of around 150 cm^{-1} can be covered and performed by scanning only the position of the delay line. For fs laser-based systems, however, an additional system may be required to compensate for higher-order dispersion and ensure a spectral resolution less than 10 cm^{-1} [13].

Funding. Co-creation place formation support program (JPMJPF2009); Core Research for Evolutional Science and Technology (JPMJCR1662); Japan Society for the Promotion of Science (21J11008).

Acknowledgments. The authors thank Dr. Hiroyuki Kawagoe of Osaka University for his technical advice on developing a laser scanning system, and Prof. Wei Min of Columbia University and Prof. Yasuyuki Ozeki of the University of Tokyo for their helpful advice on the SRS microscope. K.K is supported by JSPS Research Fellowships for Young Scientists.

Disclosures. The authors declare no conflicts of interest.

Data availability. Data underlying the results presented in this paper are not publicly available at this time but may be obtained from the authors upon reasonable request.

Supplemental document. See Supplement 1 for supporting content.

References

1. C. W. Freudiger, W. Min, B. G. Saar, S. Lu, G. R. Holtom, C. He, J. C. Tsai, J. X. Kang, and X. S. Xie, "Label-free biomedical imaging with high sensitivity by stimulated Raman scattering microscopy," Science **322**(5909), 1857–1861 (2008).
2. C. Ji-Xin and X. X. Sunney, "Vibrational spectroscopic imaging of living systems: an emerging platform for biology and medicine," Science **350**(6264), aaa8870 (2015).
3. Y. Ozeki, W. Umemura, Y. Otsuka, S. Satoh, H. Hashimoto, K. Sumimura, N. Nishizawa, K. Fukui, and K. Itoh, "High-speed molecular spectral imaging of tissue with stimulated Raman scattering," Nat. Photonics **6**(12), 845–851 (2012).
4. L. Wei, Z. Chen, L. Shi, R. Long, A. V. Anzalone, L. Zhang, F. Hu, R. Yuste, V. W. Cornish, and W. Min, "Super-multiplex vibrational imaging," Nature **544**(7651), 465–470 (2017).
5. F. Hu, C. Zeng, R. Long, Y. Miao, L. Wei, Q. Xu, and W. Min, "Supermultiplexed optical imaging and barcoding with engineered polyynes," Nat. Methods **15**(3), 194–200 (2018).
6. D. Zhang, M. N. Slipchenko, and J.-X. Cheng, "Highly sensitive vibrational imaging by femtosecond pulse stimulated raman loss," J. Phys. Chem. Lett. **2**(11), 1248–1253 (2011).
7. T. Würthwein, N. M. Lüpken, N. Irwin, and C. Fallnich, "Mitigating cross-phase modulation artifacts in femtosecond stimulated Raman scattering," J. Raman Spectrosc. **51**(11), 2265–2271 (2020).
8. M. Lai, S. T. Lai, and C. Swinger, "Single-grating laser pulse stretcher and compressor," Appl. Opt. **33**(30), 6985–6987 (1994).
9. D. Zhang, M. N. Slipchenko, D. E. Leaird, A. M. Weiner, and J.-X. Cheng, "Spectrally modulated stimulated Raman scattering imaging with an angle-to-wavelength pulse shaper," Opt. Express **21**(11), 13864–13874 (2013).

Biomedical Optics EXPRESS

10. P. Berto, E. R. Andresen, and H. Rigneault, "Background-free stimulated Raman spectroscopy and microscopy," Phys. Rev. Lett. **112**(5), 053905 (2014).
11. H. Xiong, N. Qian, Z. Zhao, L. Shi, Y. Miao, and W. Min, "Background-free imaging of chemical bonds by a simple and robust frequency-modulated stimulated Raman scattering microscopy," Opt. Express **28**(10), 15663–15677 (2020).
12. M. Andreana, M.-A. Houle, D. J. Moffatt, A. Ridsdale, E. Buettner, F. Légaré, and A. Stolow, "Amplitude and polarization modulated hyperspectral Stimulated Raman Scattering Microscopy," Opt. Express **23**(22), 28119–28131 (2015).
13. M. Mohseni, C. Polzer, and T. Hellerer, "Resolution of spectral focusing in coherent Raman imaging," Opt. Express **26**(8), 10230–10241 (2018).
14. R. L. Fork, C. H. B. Cruz, P. C. Becker, and C. V. Shank, "Compression of optical pulses to six femtoseconds by using cubic phase compensation," Opt. Lett. **12**(7), 483–485 (1987).
15. D. S. Knight and W. B. White, "Characterization of diamond films by Raman spectroscopy," J. Mater. Res. **4**(2), 385–393 (1989).
16. Y. Yonemaru, A. F. Palonpon, S. Kawano, N. I. Smith, S. Kawata, and K. Fujita, "Super-spatial- and -spectral-resolution in vibrational imaging via saturated coherent anti-Stokes Raman scattering," Phys. Rev. Appl. **4**(1), 014010 (2015).
17. M. S. Alshaykh, C.-S. Liao, O. E. Sandoval, G. Gitzinger, N. Forget, D. E. Leaird, J.-X. Cheng, and A. M. Weiner, "High-speed stimulated hyperspectral Raman imaging using rapid acousto-optic delay lines," Opt. Lett. **42**(8), 1548–1551 (2017).
18. T. E. Bridges, M. P. Houlne, and J. M. Harris, "Spatially resolved analysis of small particles by confocal Raman microscopy: depth profiling and optical trapping," Anal. Chem. **76**(3), 576–584 (2004).
19. C. Zhang, D. Zhang, and J.-X. Cheng, "Coherent Raman scattering microscopy in biology and medicine," Annu. Rev. Biomed. Eng. **17**(1), 415–445 (2015).
20. P. Samineni, B. Li, J. W. Wilson, W. S. Warren, and M. C. Fischer, "Cross-phase modulation imaging," Opt. Lett. **37**(5), 800–802 (2012).
21. A. Lombardini, P. Berto, J. Duboisset, E. R. Andresen, S. Heuke, E. Büttner, I. Rimke, S. Vergnole, V. Shinkar, P. de Bettignies, and H. Rigneault, "Background-suppressed SRS fingerprint imaging with a fully integrated system using a single optical parametric oscillator," Opt. Express **28**(10), 14490–14502 (2020).
22. S. Heuke, A. Lombardini, E. Büttner, and H. Rigneault, "Simultaneous stimulated Raman gain and loss detection (SRGAL)," Opt. Express **28**(20), 29619–29630 (2020).
23. S. Hong, T. Chen, Y. Zhu, A. Li, Y. Huang, and X. Chen, "Live-cell stimulated Raman scattering imaging of alkyne-tagged biomolecules," Angew. Chem. Int. Ed. **53**(23), 5827–5831 (2014).
24. X. Li, M. Jiang, J. W. Y. Lam, B. Z. Tang, and J. Y. Qu, "Mitochondrial imaging with combined fluorescence and stimulated Raman scattering microscopy using a probe of the aggregation-induced emission characteristic," J. Am. Chem. Soc. **139**(47), 17022–17030 (2017).
25. Y. Fu, H. Wang, R. Shi, and J.-X. Cheng, "Characterization of photodamage in coherent anti-Stokes Raman scattering microscopy," Opt. Express **14**(9), 3942–3951 (2006).
26. H. Wang, Y. Fu, and J.-X. Cheng, "Experimental observation and theoretical analysis of Raman resonance-enhanced photodamage in coherent anti-Stokes Raman scattering microscopy," J. Opt. Soc. Am. B **24**(3), 544–552 (2007).
27. T. Hellerer, A. M. Enejder, and A. Zumbusch, "Spectral focusing: High spectral resolution spectroscopy with broad-bandwidth laser pulses," Appl. Phys. Lett. **85**(1), 25–27 (2004).
28. D. Fu, G. Holtom, C. Freudiger, X. Zhang, and X. S. Xie, "Hyperspectral imaging with stimulated Raman scattering by chirped femtosecond lasers," J. Phys. Chem. B **117**(16), 4634–4640 (2013).